

Conservative Generalized Bifurcation Diagrams

Cesar Manchein^a, Marcus W. Beims^b

^aDepartamento de Física, Universidade do Estado de Santa Catarina, 89219-710 Joinville, Brazil

^bDepartamento de Física, Universidade Federal do Paraná, 81531-980 Curitiba, Brazil

Abstract

Bifurcation cascades in conservative systems are shown to exhibit a *generalized* diagram, which contains all relevant informations regarding the location of periodic orbits (resonances), their width (island size), irrational tori and the infinite higher-order resonances, showing the intricate way they are born. Contraction rates for islands sizes, along period-doubling bifurcations, are estimated to be $\alpha_I \sim 3.9$. Results are demonstrated for the standard map and for the continuous Hénon-Heiles potential. The methods used here are very suitable to find periodic orbits in conservative systems, and to characterize the regular, mixed or chaotic dynamics as the nonlinear parameter is varied.

Keywords: Conservative Systems, Bifurcations, Finite Time Lyapunov Exponent, Periodic Orbits

PACS: 05.45.Pq, 05.45.Ac

1. Introduction

Almost all physical systems in nature are so complex that long time predictions are nigh impossible. This is a characteristic of nonintegrable chaotic systems whose effects are visible in celestial mechanics, plasma physics, general relativity, quantum physics, communications problems, hard beats, social and stock market behaviors, weather forecast, among others. Thus, the precise description of the dynamics in nonintegrable systems is essential for the understanding of nature. One intrinsic and fundamental phenomenon of such nonintegrable systems, is that realistic stable orbits may vanish (or be born) when the nonlinear parameter varies. This can lead to a complicated behavior with a cascade of new orbits, which is satisfactorily described by a bifurcation diagram [1]. One example is the period doubling bifurcation (PDB) cascade, well understood in one dimensional dissipative discrete systems containing one parameter, where the intervals in the parameter, between successive PDBs, tend to a geometric progression with a universal ratio of $1/\delta = 1/4.66$, with δ being the Feigenbaum constant. For two dimensional dissipative systems, bifurcation cascades manifest themselves inside periodic stable structures in the two parameter space, which appear to be generic for a

large class of systems. Shrimp-like structures are one example, and appear in the dissipative Hénon [2, 3] and ratchet [4] discrete systems, in continuous models [5], among many others. Such structures allow an analysis of geometric approximation ratios, and provide a very clear understanding of the dissipative dynamics. In contrast to dissipative systems, for conservative nonintegrable systems the description of bifurcations cascades is much more complicated. It is known [1, 6], that by magnifying stable points in the phase space, a mixture of surrounding stable and unstable fixed points is found. This repeats itself for every stable fixed point, as explained by the Poincaré-Birkhoff theorem [7]. How higher order stable orbits bifurcate, the islands around them vary and are interconnected, and irrational tori behave as the nonlinear parameter of the system changes, is an interesting problem that still deserves to be deeply investigated. For 2 degrees of freedom area-preserving discrete systems, the intervals in the parameter between successive PDBs, tend to a geometric progression with a ratio of $1/\delta_H \sim 1/8.72$ [1]. Results have also been extended to higher-dimensional systems (please see [8, 9, 10, 11] for more details).

This work uses convergence properties of the Finite Time Lyapunov Exponent (FTLE) to explore the dynamics of conservative systems in a mixed plot: initial condition (IC) *versus* the nonlinear parameter. The location of stable orbital points is easily found in such plot, and conservative bifurcation diagrams recognized

Email addresses: cmanchein@gmail.com (Cesar Manchein), mbeims@fisica.ufpr.br (Marcus W. Beims)

to have a generalized form, containing infinite sub-diagrams with all rational/irrational tori from the periodic orbits (POs), independent of the period. This is a nice complete description, and extension, from an early work [12], done for another dynamical system. Results are remarkable and show the very complex, self-similar and generic bifurcation structure in conservative systems with only one parameter. They also suggest that contraction rates for the islands sizes, along PDBs, approach the constant $\alpha_I \sim 3.9$. A detailed numerical analysis is performed for the standard map, including the use of the first recurrence times instead the FTLEs, to demonstrate that results are independent of the method. A generalization is shown for the continuous Hénon-Heiles potential.

2. Discrete Model: The Standard Map

To start it is appropriate to present results using a well known general model with wide applications, the Chirikov standard mapping, which is given by [13]:

$$\begin{cases} p_{n+1} = p_n + (K/2\pi) \sin(2\pi x_n) \pmod{1}, \\ x_{n+1} = x_n + p_{n+1} \pmod{1}. \end{cases} \quad (1)$$

K is the nonlinearity parameter and x_n, p_n are respectively position and momentum at discrete times $n = 1, 2, \dots, N$. It is known that period-1 (shortly written per-1) fixed points are $p_1 = 1/2m$ (m integer) and $x_1 = 0, \pm 1/2$. The point $x_1 = 0$ is always unstable while $x_1 = \pm 1/2$ becomes unstable for $K > 4$. There exist also per-1 fixed points related to accelerator modes [13] whose stability condition is $|2 \pm K \cos x_{1l}| < 2$, with $K \sin x_{1l} = 2\pi l$ and l integer. For higher periods there are primary families of periodic points (which exist in the limit $K \rightarrow 0$) and bifurcation families which are born only for larger values of K (See [1] for more details).

3. Method: Finite Time Lyapunov Exponents

The key idea for the success of our proposal is the observation that the numerical convergence of the FTLEs is *distinct* for different ICs (same nonlinear parameter K), even between regular trajectories. To make this clear, consider, for example, that the IC is exactly on the stable (for $K \leq 4$) fixed point $x_0 = 1/2$. It can be calculated analytically that the corresponding Lyapunov exponent (LE), after one iteration, is exactly zero. But now consider that we start with an IC close to this fixed point, say $x'_0 = 1/2 + \Delta x_0$, which can be an irrational regular

torus close to x_0 . Assuming that $(\Delta x_0)^2 \approx 0.0$, the standard map can be linearized around x'_0 and the FTLE determined analytically, after n iterations, from the eigenvalues of the composed Jacobian $\{(1, -K), (1, 1 - K)\}^n$. This FTLE is plotted in Fig. 1(a) as a black continuous line, and it converges exactly to zero only when $n \rightarrow \infty$. This means that ICs from stable tori around the fixed point, take a longer time to converge exactly to zero than the fixed point itself. This behavior can also be observed numerically by determining the FTLEs using Benettin's algorithm [14, 15], which includes the Gram-Schmidt re-orthonormalization procedure. We use the six exemplary orbits shown in the inset of Fig. 1(a): the stable fixed point, demarked with a cross, and the five irrational tori around the fixed point. All trajectories are regular and have LEs exactly equal zero for infinite times. However, when calculating the FTLEs for the distinct ICs, we observe that ICs closer to the fixed point converge faster to zero. In Fig. 1(a), the decay curves for the FTLEs *versus* times are plotted (starting from below) for the six ICs shown in the inset (starting from the fixed point). As ICs are taken more away from the periodic point, FTLEs converge slower to zero. The magnitude of the FTLEs between different irrational tori are really small and not significant for any purpose. However, for the IC exactly on the PO, the FTLE converges faster to zero than other ICs around it. Essential to mention is that this is not a numerical convergence artefact due to the numerical method, but an analytical property, as shown above (continuous line in Fig. 1(a)). Thus,

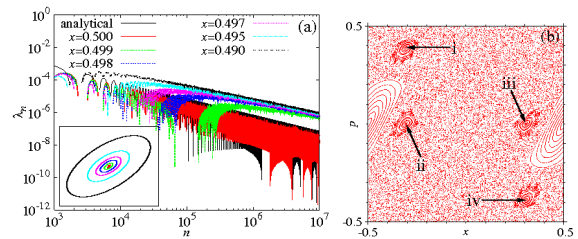


Figure 1: (Color online) (a) Log-log plot of the FTLEs (starting from below) as a function of the iteration time for the six trajectories shown in the inset (starting from the fixed point), and (b) phase space for $K = 2.6$.

even though such small FTLEs are insignificant to distinguish between the irrational tori, they allow us to recognize where POs are *located* in phase space, and to understand the very complex and self-similar behaviors, which occur close to the POs as the nonlinear parameter K changes. For larger times, FTLEs in Fig. 1(a) continue to decrease linearly to zero, until the machine precision is reached, and when the actual method can-

not be used anymore. Even though the method was explained using the standard map, it is equally applied to other conservative dynamical systems.

4. The Generalized Diagrams

Using the properties explained in Section 3, a very clarifying plot can be constructed, which allows us to recognize the bifurcation diagram in conservative systems in a simple way. Figure 2 shows the FTLE (see colors bar) in the mixed space $x_0 \times K$ with $p_0 = 0.0$. Black lines are related to those ICs for which the FTLEs converge faster to zero and POs exist (this was checked explicitly for many black lines). Dark to light yellow points, around the main black lines, are related to irrational tori and also define the size of the corresponding island. These are regular trajectories for which the associated FTLEs are still not that close to zero, as those FTLEs from ICs which start exactly on the black lines (POs). For $n \rightarrow \infty$ these points also become black. Light yellow, blue to red points, are ICs related to chaotic trajectories. Clearly we observe that the fixed

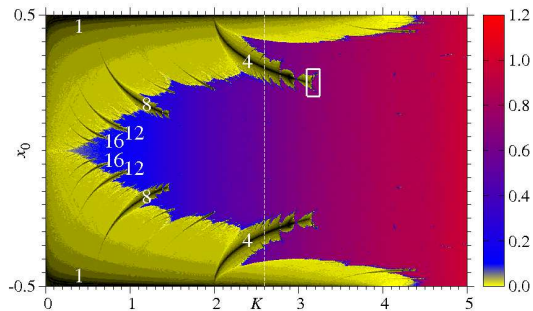


Figure 2: (Color online) FTLEs in the mixed space $x_0 \times K$ for the standard map with $p_0 = 0.0$, a grid of $10^3 \times 10^3$ points and 10^4 iterations.

point $x_0 = x_1 = 0.0$ is unstable (positive FTLEs along the line $x_0 = 0.0$) for any K value. In the chaotic region, FTLEs increase monotonically with K and the dynamics is not much exciting. However, in the regular to chaotic transition region, trajectories combine themselves in a very complicated way, bifurcations occur and the dynamics is very rich as K changes. For clarification, Fig. 1(b) shows the corresponding phase space dynamics for $K = 2.6$ [see white dashed line in Fig. 2]. One per-1 (at $x = \pm 0.5, p_0 = 0.0$) and one per-4 (see numbers i, ii, iii, iv showing the orbital points) POs are shown. The per-1 orbital points correspond to the black points in Fig. 2 located at $x_0 = \pm 0.5$ and $K = 2.6$. This is the primary resonance. The two orbital points (ii,iii), from the per-4 PO, belong to the black curves in Fig. 2.

Since we always started along the initial line $p_0 = 0.0$, Fig. 2 is able to detect only the two orbital points (ii,iii) along this line. The whole dark to yellow region around $x_0 \pm 0.5$ (for $K \leq 4$) in Fig. 2, gives the island size and is related to all irrational tori around this PO.

ICs which leave to stable POs (black lines), are characterized by the “Christmas tree” structure around it. For example, for $K = 2.0$ in Fig. 2, two per-4 trees are born, one at $x_0 = -0.5$, and the other one at $x_0 = 0.5$. All trees have a main “stem” in the center, which is black and gives the location of the stable PO when K varies. Since both mentioned trees are born from $x_0 = \pm 0.5$, they are secondary resonances with per-4. A sequence of identical trees (secondary resonances) with smaller and smaller sizes, and increasing periods 8, 12, 16, ... [see numbers on the sequence of trees Fig. 2], are observed by decreasing K . The stem of these trees, which are all born from the PO $x = \pm 0.5$, are related to the rational tori. The width of the tree is the width of the island along the line $p_0 = 0.0$. In addition, these trees approach to each other as they get closer to the unstable fixed point at $x_0 = 0.0$ and $K \rightarrow 0.0$. A large sequence of approximating trees is also observed (not shown here) close to $K \sim 4.0$ (where the per-1 PO becomes unstable) and $x_0 \rightarrow \pm 0.5$. The main stems

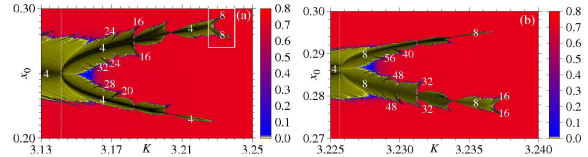


Figure 3: Magnifications of (a) the per-4 fork from the box from Fig. 2 and (b) per-8 fork from box from (a). Numbers indicate the periods of the POs.

in the above trees exist until they become unstable at the very end of the tree (on the right), where a pitchfork bifurcation occurs. This is better visualized in the magnification shown in Fig. 3(a) which, roughly speaking, summarizes results contained in Figs.7 and 8 from [12], obtained for another dynamical system. However, Fig. 3(a) contains many essential additional informations about the rich underline dynamics, as described below. The main stem (stable PO) becomes unstable close to $K \sim 3.145$ and $x_0 \sim 0.25$, as can be recognized by the yellow points (see dashed line). Simultaneously around this point, two black lines (stable POs) are born with the same per-4, characterizing the pitchfork bifurcation. In fact, a “fork”-like structure (diagram) is born at the bifurcation point and contains two new main trees. This fork is the *generalized diagram*, which lives in the *entire* portion of the mixed plot where the *tran-*

sition from regular to chaotic motion occurs. This was checked for many other magnifications, even for higher order periods. Since the interesting dynamics and all bifurcation processes occur through the fork and its trees, it is enough to discuss just one fork to understand the very rich dynamics from the whole Fig. 2.

For this we start discussing the magnification of the per-4 fork shown in Fig. 3(a). Inside one fork, two main trees always exist: one called the Line Tree (LT), where PDBs occur for ICs *on* the line $p_0 = 0.0$; and the other is the Outline Tree (OT), where PDBs occur for ICs *outside* $p_0 = 0.0$. In the example from Fig. 3(a), the OT is the lower one and the LT is the upper one, which is identical to all secondary trees shown in Fig. 2. LT and OT have a main stem related to *distinct* POs, but with the *same* period [see the numbers in Fig. 3(a)]. Emerging almost perpendicularly from the main stems, infinite smaller sub-trees are born below and above. Such new sub-trees have also a main stem related to another PO with higher period. In the ramifications shown in Fig. 3(a), the new POs emerging from the LT, as K decreases, are: 8(new fork, see box), 16, 24, 32, ... while for the OT are: 20, 28, 36, ... These new ramifications (sub-trees) are the rational tori (higher-order resonances) which live around the per-4 point. At the end of the fork (on the right), the main stems from the LT and OT suffer a PDB phenomenon. This is shown in details in Fig. 3(b), which is a magnification of the white box per-8 fork from Fig. 3(a). Besides the new trees emerging from the main stem, a continuous transition to lighter colors occurs when we go away from the main stem, in the direction of the border of the tree. All these points are related to irrational tori around the main PO. At the border of all trees, the breakdown of the last irrational torus, of the corresponding PO, can be observed by the transition from yellow to red points, where positive FTLEs appear and the dynamics becomes chaotic. Remarkable is that the dynamics around this new unstable point, as K increases, is similar to the dynamics around the unstable per-1 ($x_0 = 0.0$) orbit, observed in Fig. 2 for K close to zero. Collecting the main properties of the generalized fork, suppose it has a per- q for the main stems of the LT and OT. The ramifications have distinct periods, namely for the LT we have, starting from the right border of the fork: $2q$ (new fork), and the ramifications related to the rational tori have periods $4q, 6q, 8q, \dots$. For the OT we have $2q$ (not seen along the line $p_0 = 0.0$) with the ramifications $5q, 7q, 9q, \dots$. From successive magnifications (not shown) of the generalized fork, we found that it contracts with a ratio $\delta_F \sim 8.7$, and that the islands sizes, at the PDBs, approach the estimated

contraction rate $\alpha_I = d_q/d_{2q} \sim 3.90 \pm 0.04$, where d_q is the island size for $q = 128$. In order to estimate d_q , we magnified the forks with main periods $q = 128$ and 256 , using times $n = 10^9$. For such times, the border line between the last irrational tori around the POs and the chaotic motion becomes evident, and d_q can be determined from the numerical data of the FTLEs.

5. A continuous model

The general statement of our results can be confirmed showing the existence of trees in the continuous Hénon-Heiles (HH) potential $V(x, y) = (x^2 + y^2)/2 + x^2y - y^3/3$. It is a truncation of the Toda potential [1] used in celestial mechanics and extensively mentioned as a benchmark to nonlinear conservative dynamics. In this case the

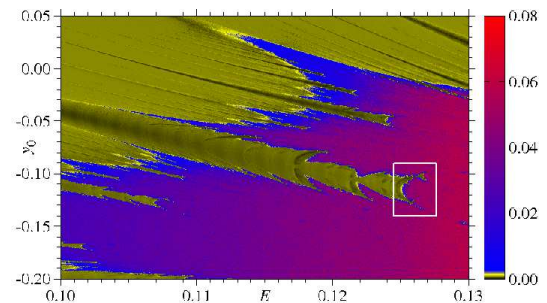


Figure 4: FTLE in the space $E \times y_0$ for the HH potential with $x_0 = p_{y_0} = 0.0$, while p_{x_0} is obtained from energy conservation.

nonlinear parameter is the total energy E . For $E = 1/24$ the dynamics is regular, and when $E \rightarrow 1/6$ it becomes mixed and finally chaotic. Figure 4 shows the FTLEs in a portion of the mixed plot $E \times y_0$ for the HH problem. As in Fig. 2, black lines are related to those ICs which leave to close to zero FTLEs, where POs are present. Dark to yellow colors are related to the rational/irrational tori. Clearly we observe the existence of the stable trees, the forks (see white box for one example) and the infinite sequence of trees ramifications (higher order resonances), always appearing in form of the tree described in details for the standard map.

6. Changing the method: First recurrence times

The purpose of this section is to show that the generalized diagrams can be obtained using another method. Despite results using the FTLEs are totally trustworthy, it is proper to use a distinct method. For this we reproduce Fig. 2 using the first recurrence times (FRTs) instead the FTLEs. We start the simulation with ICs inside

the interval $-0.5 < x_0 < 0.5$, $p_0 = 0.0$, iterate the standard map (1) and reckon $\Delta x_n = x_0 - x_n$, $\Delta p_n = p_0 - p_n$. When $|\Delta x_n| < 10^{-4}$ and $|\Delta p_n| < 10^{-4}$, we record $T_1 = n$. For $n > T_{max} = 10^4$ we stop the simulation. In this way we compute the number of iterations T_1 , which a given trajectory needs to come back to the initial point (inside a circle of radius 10^{-4}) for the first time. It is expected that for POs the time T_1 is smaller (equal to the period of the orbit), and that for chaotic trajectories the limit $n = T_{max}$ is reached. In between, all values of T_1 are possible, and are usually related to irrational tori or POs with very large periods. Results are shown in

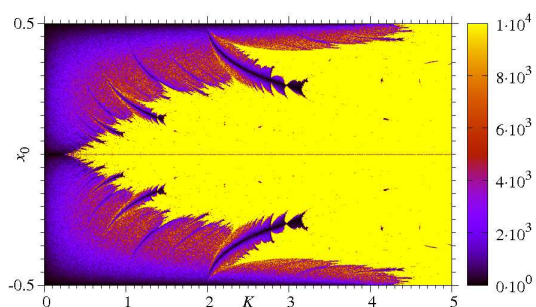


Figure 5: FRT T_1 (see color bar) for the standard map (1) in the plot ICs *versus* K .

Fig. 5. Plotted is T_1 (see color bar) as a function of ICs x_0 and K . Black points are related to smaller times and are identified as the POs. Purple to red points are the irrational tori with intermediate values of T_1 . Yellow points are related to chaotic trajectories, which never returned (for $n \leq 10^4$) to the IC. Even though Fig. 5 is plotted with different colors, all trees, forks structures, widths and scalings, are identical to Fig. 2. In addition, the FRTs are able to find the location of *unstable* POs, as for example, the straight horizontal line at $x = 0.0$, which is the unstable fixed point for any K .

The reason why the FRTs work so well to reproduce the results from the FTLEs is a discussion which we cannot explore in a satisfactory way in this work. It has also other important properties. The main point here is to demonstrate that our results are real physical effects, relevant and independent on the method: FTLEs, FRTs, or any other quantity whose time convergence is affected by the ICs.

7. Conclusions

To conclude, period doubling bifurcations in conservative systems are shown to exhibit a generalized stable diagram in the plot: initial conditions *versus* the nonlinear parameter. This diagram is composed of two main

trees whose main stems are the periodic orbits (resonances) and infinite ramifications, which are all rational tori (higher-order resonances) surrounding the periodic orbits. Results are discussed in details for the standard map and extended to the continuous Hénon-Heiles potential. The generalized trees were also confirmed to exist (not shown), for the nontwist standard map [16] and the hydrogen atom subjected to an external magnetic field [17], and can be recognized in [12], giving additional evidences about their wide applicability in conservative systems. First recurrence times and finite time Lyapunov exponents were used for the standard map, showing that results are independent of the method. Other methods could be used to find the trees as, for example, the finite time rotation numbers. This is what Fig. 5, from the recent work about the nontwist standard map [18], suggests, providing one more example of a distinct system, with another method, where the generalized diagram should appear. Our results are also independent of the periods of the periodic orbits, and provide general clues for conservative systems concerning: the regular/mixed/chaotic dynamics, the location of stable orbital points, the generic mechanism of bifurcation phenomenon, and that contraction rates of islands sizes, along period doubling bifurcations, follow $\alpha_I \sim 3.9$. To finish, from the present analysis it is possible to conjecture that, for higher dimensional systems, the dynamics outside the generalized bifurcation diagram, and for small nonlinearities, should produce Arnold stripes [19], which display the ICs from the stochastic Arnold web as a function of the nonlinearity parameter.

8. Acknowledgments

The authors thank FINEP (under project CTINFRA-1) and MWB thanks CNPq for financial support.

References

- [1] A.J.Lichtenberg, M.A.Lieberman, Regular and Chaotic Dynamics, Springer-Verlag, 1992.
- [2] J.A.C.Gallas, Phys.Rev.Lett. **70** (1993) 2714.
- [3] S.Hayes, C.Grebogi and E.Ott, Phys.Rev.Lett. **70** (1993) 3031.
- [4] A.Celestino, C.Manchein, H.A.Albuquerque and M.W.Beims, Phys.Rev.Lett. **106** (2011) 234101.
- [5] C.Bonato and J.A.C.Gallas, Phys.Rev.E **75** (2007) R055204.
- [6] L.E.Reichl, The Transition to Chaos, Springer-Verlag, Berlin, 2004.
- [7] E.Ott, Chaos in dynamical systems, Cambridge, 2002.
- [8] T.Bountis and R.H.G.Helleman, J.Math.Phys. **22** (1981) 1867.
- [9] R.H.G.Helleman, Phys.Rev.A **35** (1987) 1847.
- [10] J.M. Mao, J.Phys.A **21** (1988) 3079.
- [11] S-Y.Kim, Phys.Rev.E **50** (1994) 4237.

- [12] J.M.Greene, R.S.Mackay, F.Vivaldi and M.J.Feigenbaum, *Physica* 3D (1981) 468.
- [13] B.V.Chirikov, *Phys.Rep.* **52** (1979) 263.
- [14] G.Benettin, C.Cercignani, L.Galgani, and A.Giorgilli, *Lett.Nuovo Cimento* **29** (1980) 163.
- [15] A.Wolf, J.B.Swift, H.L.Swinney and J.A.Vastano, *Physica D* **16** (1985) 285.
- [16] J.D.Szezech, I.L.Caldas, S.R.Lopes, R.L.Viana and P.J.Morrison, *Chaos* **19** (2009) 043108.
- [17] M.W.Beims and J.A.C.Gallas, *Phys.Rev.A* **62** (2000) 043410.
- [18] J.D.Szezech, Jr., I.L.Caldas, S.R.Lopes, P.J.Morrison and R.L.Viana, *Phys.Rev.E* **86**, 036206 (2012).
- [19] M.S.Custódio, C.Manchein and M.W.Beims, *Chaos* **22**, 026112 (2012).